Inorganic Chemistry
Cite This: Inorg. Chem. 2019, 58, 2770−2776
Article
pubs.acs.org/IC

Structure and Transport Properties in Itinerant Antiferromagnet $RE_2(Ni_{1-x}Cu_x)_5As_3O_2$ (RE = Ce, Sm)

Xu Chen,[†,‡] Jian-gang Guo,*[,†,§] Chunsheng Gong,[†] Erjian Cheng,[∥] Yanpeng Song,[†,‡] Tianping Ying,[∥] Jun Deng,[†,‡] Shiyan Li,[∥,#] and Xiaolong Chen*[,†,§]

[†]Beijing National Laboratory for Condensed Matter Physics, Institute of Physics, Chinese Academy of Sciences, P.O. Box 603, Beijing 100190, China

[‡]University of Chinese Academy of Sciences, Beijing 100049, China

[§]Songshan Lake Materials Laboratory, Dongguan, Guangdong 523808, China

[∥]State Key Laboratory of Surface Physics, Department of Physics, and Laboratory of Advanced Materials, Fudan University, Shanghai 200433, China

[#]Collaborative Innovation Center of Advanced Microstructures, Nanjing 210093, China

Supporting Information

ABSTRACT: We report the crystal structure and physical properties of two Ni_5As_3-based compounds $RE_2Ni_5As_3O_2$ (RE = Ce, Sm). The former exhibits structural phase transition from tetragonal (space group *I*4/*mmm*, 139) to orthorhombic (space group *Immm*, 71) symmetry at 230 K, while the latter undergoes a charge-density-wave-like structural distortion with abrupt change of Ni−As bond length. Both compounds show antiferromagnetic transitions due to RE^{3+} ions ordering at 4.4 and 3.4 K, accompanying with the large enhancement of Sommerfeld coefficients comparing to the nonmagnetic La analogue. Although the Cu substitution for Ni induces structural anomalies and suppression of structural transition like the behaviors in La/Pr/Nd analogues, the superconductivity is not observed in both Cu-doped $RE_2Ni_5As_3O_2$ (RE = Ce, Sm) above 0.25 K. Our structural refinements reveal that the lacking of superconductivity in $RE_2(Ni_{1-x}Cu_x)_5As_3O_2$ might relate to the anomalous increase of As height, h_1.

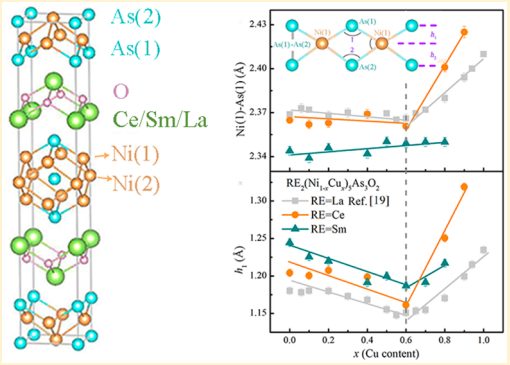

INTRODUCTION

Identifying the key structural unit and tuning its geometry are important in exploring superconductor and understanding the relationship between superconductivity (SC) and crystal structure. One known example is FeAs-based superconductors, in which the distorted degree of $FeAs_4$ tetrahedral empirically determines the highest superconducting critical temperature (T_c), magnetism, and correlation strength.[1−3] Replacing the La_2O_2 layer by Sm_2O_2 can effectively enhance the T_c from 26 to 58.1 K by optimizing the $FeAs_4$ tetrahedral geometry.[4−7] Actually, the inherent mechanism is mainly tuning an indirect hybridization degree of Fe d_{xz}/d_{yz} orbital and As p_z orbital, which can make the regular shape of $FeAs_4$ tetrahedral (Fe−As−Fe angle: 109.5°; As height:1.38 Å) have optimal electron-correlation strength and hopping exchanges.

Besides, the anionic cluster of $(Ch_2)^{2-}$ (Ch = Se, Te) and $(Pn_2)^{4-}$ (Pn = P, As) can be viewed as novel carrier controlling unit,[8−10] in which the main group elements are connected by covalent bond. Altering the bond length can change the total electron numbers and structural stability, which synergistically influences the carrier concentration and electron−phonon coupling strength. Previous experiments demonstrated that elongating the bond length of $(Ch_2)^{2-}$ dimer could significantly enhance the T_c and change the crystal structure. For example, in pyrite-type Ir_xSe_2, increasing Ir content can lengthen the bonds of Se−Se and simultaneously influence the T_c.[11,12] The maximal T_c of 10 K can be reached as the weakest Se−Se bonding states and the structural instability emerges.[11] Similarly, the breaking of Te−Te bonds in $AuTe_2$ by chemical substitution and physical pressure could induce SC accompany with a phase transition.[13,14] Furthermore, As^-−As^- zigzag chain and As−As dimer are observed in $Ca_{1-x}La_xFe_2As_2$[15,16] and Pt−$CaFe_2As_2$,[17,18] respectively, which are critical to stabilize the crystal and SC.

Very recently, three series of $RE_2(Ni_{1-x}Cu_x)_5As_3O_2$ (RE = La, Pr, Nd) superconductors were discovered by us,[19] in which a Ni_5As_3 unit composed of antifluorite Ni_2As_2 layer and two As−As dimer is believed to be the critical ingredient for SC. It is found that Cu doping could enhance the T_c to 2.5 K. It offers an opportunity to study the evolution of Ni_5As_3 unit and SC through tuning the geometry of $NiAs_4$ polyhedral and As

Received: December 3, 2018
Published: January 25, 2019

DOI: 10.1021/acs.inorgchem.8b03360
Inorg. Chem. 2019, 58, 2770−2776

height. In this work, we report that the structure and properties of two analogous $RE_2(Ni_{1-x}Cu_x)_5As_3O_2$ (RE = Ce, Sm), which exhibit structural transition or charge-density-wave-like distortion under low temperatures. Through Cu doping, however, the SC is not observed as low as 0.25 K in all measured samples. Combing the crystallographic parameters in all five $RE_2(Ni_{1-x}Cu_x)_5As_3O_2$ compounds, the evolution of Ni_5As_3 unit has been systemically investigated, and the optimal geometry of Ni_5As_3 unit is identified.

EXPERIMENTAL SECTION

Polycrystalline samples of $RE_2(Ni_{1-x}Cu_x)_5As_3O_2$ (x = 0.0−1.0) were synthesized by solid-state reactions. The binary precursors CeAs/SmAs, Cu_3As and NiAs were presynthesized by reacting Ce/As filings, Cu, Ni, and As powders at 1000 K for 20 h. Then, the powders of CeAs/SmAs, Cu_3As, NiAs, La_2O_3/Sm_2O_3, Ni and Cu were weighted as the stoichiometric ratio, ground and pelleted under a pressure of 15 MPa in an argon-filled glovebox. The pellets were loaded into an Al_2O_3 crucible and sealed into evacuated silica tube, which was heated up to 1250 K and kept for 40 h. The powder X-ray diffraction (PXRD) pattern was collected at room temperature using a Panalytical diffractometer (Cu Kα radiation) equipped a low-temperature option (10−300 K). Rietveld refinements were performed using Fullprof suites.[20] The electrical resistivity (ρ), dc magnetic susceptibility (χ), and heat capacity (C_p) were measured through the standard four-wire method, vibrating sample magnetometer and heat relaxation method at PPMS (Quantum Design), respectively. The resistance below 1.8 K was measured in an Oxford fridge equipped with a dilution refrigerator and a He-3 probe. Crystal orbital Hamilton population (COHP) analysis as implemented in the LOBSTER package[21,22] gives information about the interatomic interaction, where a negative (positive) COHP value indicates bonding (antibonding) states.

RESULTS AND DISCUSSION

Figure 1a,b shows the Rietveld refinements of PXRD pattern of $RE_2Ni_5As_3O_2$ (RE = Ce, Sm) collected at 300 K, respectively. The calculated profiles are based on the initial model $RE_2Cu_5As_3O_2$.[19] Two refinements converged to R_p = 2.17% and R_{wp} = 3.00%, R_p = 1.99% and R_{wp} = 2.76%, respectively, indicating the reliable structural determination. The lattice constants of $Ce_2Ni_5As_3O_2$ are $a = b$ = 4.0360(1) Å, c = 22.3686(5) Å with space group $I4/mmm$ (No. 139), and those of $Sm_2Ni_5As_3O_2$ shrink to $a = b$ = 3.9738(1) Å, c = 22.3053(6) Å due to the smaller ion radius of Sm^{3+}.[23,24] The crystal structure of $RE_2Ni_5As_3O_2$ (RE = Ce, Sm) are drawn as inset of Figure 1a, which is consisted of fluorite-type RE_2O_2 layer and Ni_5As_3 unit. The Ni_5As_3 can be viewed as conjunction of two antifluorite Ni_2As_2 layers through Ni−Ni metallic bonds (2.60 Å). Here, the As(1)−As(2) distances along the c-axis (2.68 and 2.73 Å) locate the bonding regime of As−As covalent bonds, and the As(1)−As(2) bond length determines the thickness of Ni_5As_3 unit along c-axis.

The temperature-dependent electrical resistivity (ρ-T) of $Ce_2Ni_5As_3O_2$ is plotted in Figure 2a. It shows typical metallic behavior, where two resistivity kinks at T_s = 230 K and T_N = 4.4 K are observed. The former is associated with the structural phase transition like the observation in ref 19, and the latter is believed to be an antiferromagnetic transition of Ce^{3+} ion. To check the structural phase transition, we measured the low-T PXRD patterns of $Ce_2Ni_5As_3O_2$ from 300 to 10 K (see Figure S1). Figure 2b shows the Rietveld refinements of PXRD profile of $Ce_2Ni_5As_3O_2$ at 10 K, in which the structure symmetry lowers to $Immm$ (No. 71) with a_0 = 4.0315(1) Å, b_0 = 4.0608 (1) Å and c = 22.1875 (2) Å, exhibiting a rotation breaking

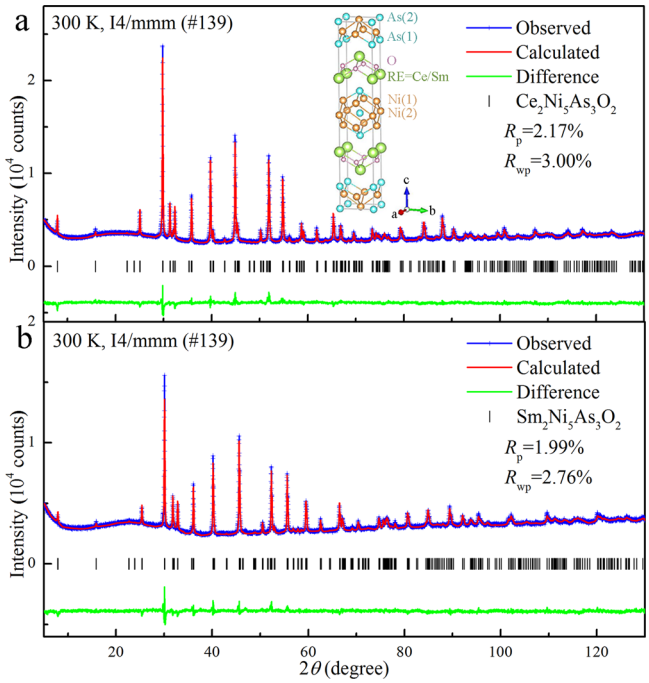

Figure 1. Rietveld refinements of powder X-ray pattern of $Ce_2Ni_5As_3O_2$ (a) and $Sm_2Ni_5As_3O_2$ (b) collected at 300 K. The inset of (a) is crystal structure of $RE_2Ni_5As_3O_2$.

(C_4−C_2). The inset of Figure 2b shows the schematic structure of Ni_4As unit at 10 K. The Ni−Ni square plane changed into distorted Ni_4As polyhedral with two upshifted Ni(1) and two downshifted Ni(2). In Figure 2c, we found that the (105) and (200) peaks split into (015)/(105) and (020)/(200) peaks below 220 K. The resultant lattice constants are shown in Figure 2d. It can be seen that the symmetry breaking and the abrupt changes in c and volume (V) clearly evidence a structural phase transition as temperature going through 230 K.

The temperature-dependent magnetic susceptibility (χ−T) of $Ce_2Ni_5As_3O_2$ is plotted at Figure 3a. The structural-transition induces a small drop in $1/\chi$ at 230 K. The data from 80 to 210 K can be well fitted by modified Curie−Weiss equation $1/\chi = (T - \theta)/C$, where C is a materials-specific Curie constant and θ is Curie temperature. The estimated magnetic moment is ∼2.94 μ_B and θ = −27 K, indicating an AFM interaction due to RE^{3+} ions ordering, which is often observed in the layered compounds with $[RE_2O_2]^{2+}$ layers.[24] A little downward in $\chi(T)$ curve is found below ∼4.2 K, which is a hint of AFM transition. In Figure 3b, we plotted the specific heat (C_p) of $Ce_2Ni_5As_3O_2$ from 270 to 2.0 K, in which a sharp peak shows up at 230 K, perfectly matching the temperature of phase transition. The sharp peak indicates that it is a first-order transition. Furthermore, fitting of low-temperature data using the equation $C_p/T = \gamma + \beta T^2 + \eta T^4$ gives Sommerfeld coefficient (γ) is 93.6 mJ/mol K^2, β = 1.18 mJ/mol K^4, and η = 1.8 × 10^{-4} mJ/mol K^6. The Debye temperature (Θ_D) is estimated to be 270.2 K as the equation $\Theta_D = (12\pi^4 nR/5\beta)^{1/3}$. Meanwhile, we noted there is a large upturn of $C_p(T)$ below 5 K, which is attributed to AFM ordered transition of Ce 4f electron spin rather than that of Ni.[25,26] The extrapolated $\gamma(0)$ of 0 K is about 15 J/(mol K), which comes from the strong interaction of Ce 4f and Ni 3d electron.

DOI: 10.1021/acs.inorgchem.8b03360
Inorg. Chem. 2019, 58, 2770−2776

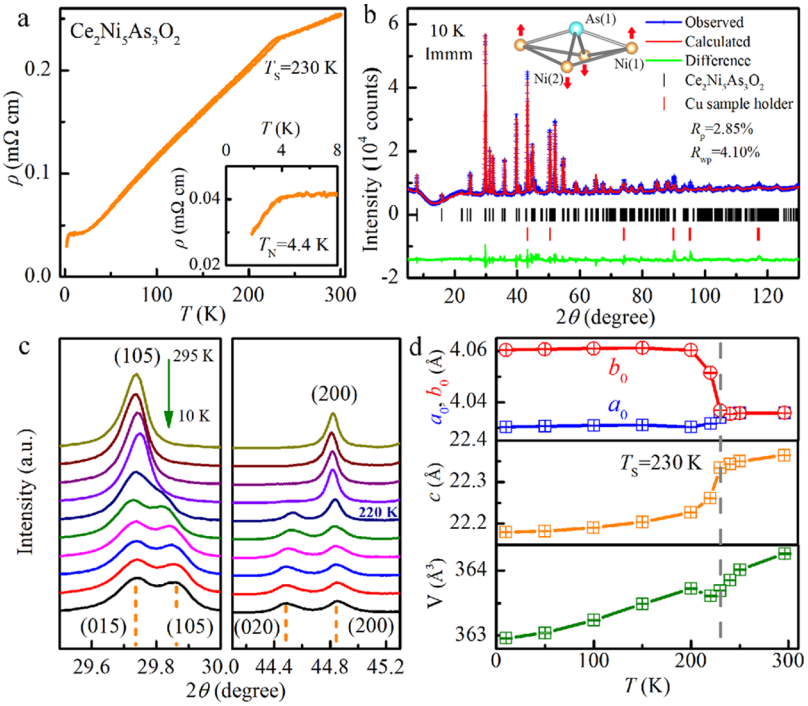

Figure 2. (a) Electrical resistivity (ρ) of $Ce_2Ni_5As_3O_2$ as a function of temperature from 2 K-300 K. Inset is the $\rho(T)$ data in lower-temperature range. (b) Rietveld refinements of powder X-ray pattern of $Ce_2Ni_5As_3O_2$ collected at 10 K. Inset is the distortion of Ni_4As polyhedral below T_s. (c) Splitting of (105) and (200) peaks at different temperature. (d) Temperature-dependent lattice constants of $Ce_2Ni_5As_3O_2$.

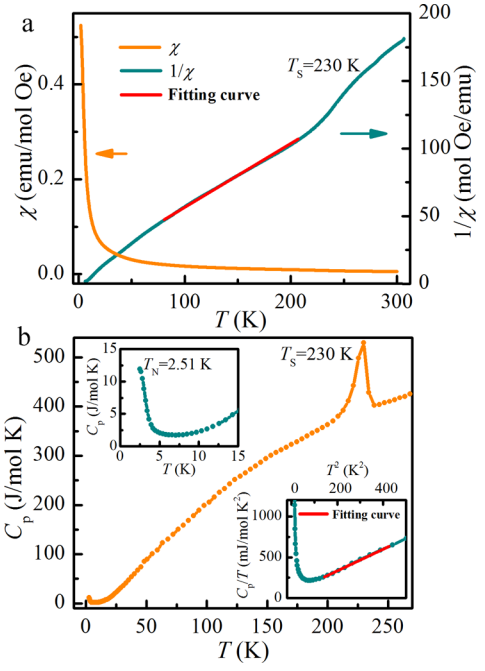

Figure 3. (a) Temperature-dependent magnetic susceptibility and the fitting results of $Ce_2Ni_5As_3O_2$. (b) The specific heat (C_p) of $Ce_2Ni_5As_3O_2$ from 270 to 2 K. The insets show expanded view and the fitting curve in low-temperature range.

The $\rho-T$ curve of $Sm_2Ni_5As_3O_2$ is shown in Figure 4a. Besides the metallic behavior, we observe a large jump of resistivity at T^* = 80 K and small increase at T_N = 4.05 K. The hysteresis of jump implies that it is a first-order transition. Meanwhile, the Hall coefficient (R_H), shown as inset of Figure 4a, changes from positive to negative below ~80 K, indicating that the Fermi surface is dominated by electrons after this transition. Similarly, the PXRD pattern at 10 K of $Sm_2Ni_5As_3O_2$ is refined to check the insight of resistivity jump (see Figure S2). Figure 4b is the Rietveld refinements profile of $Sm_2Ni_5As_3O_2$. In contrast to that of $Ce_2Ni_5As_3O_2$, this pattern is still well-refined by a tetragonal unit cell (space group: $I4/mmm$) without lowering rotation symmetry. The whole fitting converged to R_{wp} = 4.59% and R_p = 3.04%. In Figure 4c, upon cooling, the lattice constant, a, monotonously decreases, while c increases and tends to saturate below 150 K, showing a small kink at 80 K. This anomalous variation in lattice constants is totally different from what happened in the $RE_2TM_5As_3O_2$ (TM = Cu, Ni).[19] Carefully examining the low-temperature structure, we found that an increase of c, 0.05%, is mainly attributed to the increase of As(1)−As(2) bond length (1.3%), see Figure 4d. Actually, in the Ni_5As_3 unit, the two kinds of anion height (h_1 and h_2) show inversed trend by cooling, i.e., the upper h_1 increases and the lower h_2 decreases (see Figure S3). It means that the value of coordination of $z_{Ni(1)}$ will continuously decrease, what perfectly matches our Rietveld refinements as shown in Figure 4e,f. Furthermore, there is an abrupt drop of $z_{Ni(1)}$ at 80 K, which is believed to be a kind of weak charge-density-wave-like transition as observation in KNi_2S_2.[27]

The temperature-dependent magnetic susceptibility ($\chi-T$) of $Sm_2Ni_5As_3O_2$ is plotted at Figure 5a. A clear AFM transition has been detected at T_N = 4.11 K, which confirms that the increase of $\rho(T)$ is due to formation of magnetic ordering of Sm^{3+} ions. The $1/\chi-T$ data is fitted by modified Curie−Weiss equation, yielding magnetic moment (μ_{eff}) is ~1.21 μ_B and θ = −15 K. The scale of μ_{eff} is slight smaller than the theoretical value of free Sm^{3+} ions. In Figure 5b, we plotted the specific heat (C_p) of $Sm_2Ni_5As_3O_2$ from 120 to 2.0 K. We did not see any anomaly around T^* = 80 K. In the lower temperature

DOI: 10.1021/acs.inorgchem.8b03360
Inorg. Chem. 2019, 58, 2770−2776

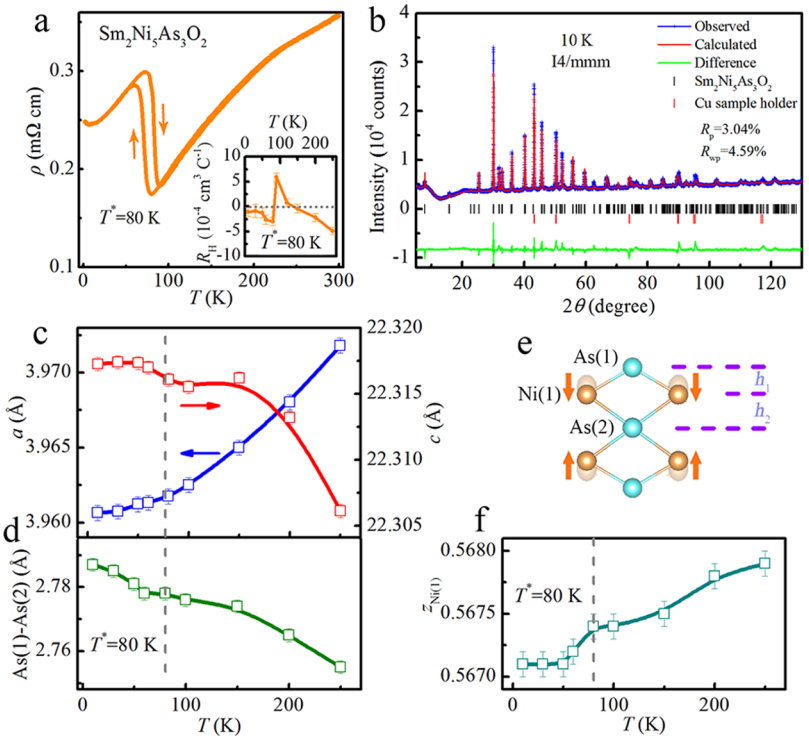

Figure 4. (a) Electrical resistivity (ρ) of $Sm_2Ni_5As_3O_2$ as a function of temperature from 2 to 300 K. Inset is the temperature dependence of Hall coefficient $R_H(T)$. (b) Rietveld refinements of powder X-ray pattern of $Sm_2Ni_5As_3O_2$ collected at 10 K. (c) and (d) Temperature-dependent lattice constants and As(1)−As(2) bond lengths of $Sm_2Ni_5As_3O_2$. (e) Schematic evolution of NiAs fragment below 80 K. (f) Temperature-dependent atomic site of $z_{Ni(1)}$.

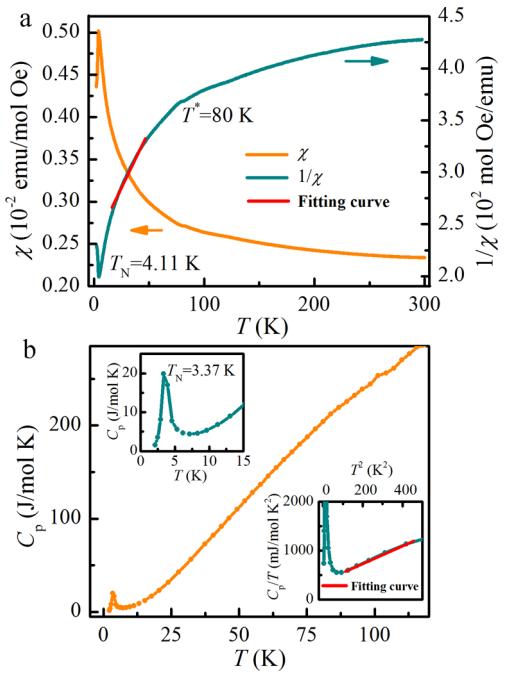

Figure 5. (a) Temperature-dependent magnetic susceptibility and the fitting results of $Sm_2Ni_5As_3O_2$. (b) Specific heat (C_p) of $Sm_2Ni_5As_3O_2$ from 120 to 2 K. Insets show the low-temperature C_p and C_p/T vs T and their fitting curves.

range, a well-defined peak has been observed at 3.37 K, which is consistent with the temperature of AFM ordering of Sm^{3+} ions. Fitting the low-temperature data using equation, $C_p/T = \gamma + \beta T^2 + \eta T^4$, yields the Sommerfeld coefficient (γ) is 362.7 mJ/mol K^2, β = 1.97 mJ/mol K^4, and $\eta = 3.1 \times 10^{-4}$ mJ/mol K^6. Adding the contribution of ηT^4 can better fit the data, implying that small anharmonic effect due to anisotropic bonding states may exist. The Debye temperature (Θ_D) is estimated to be 228.3 K as the equation $\Theta_D = (12\pi^4 nR/5\beta)^{1/3}$, which is a little smaller that of $Ce_2Ni_5As_3O_2$. These observations are like the behaviors of Kondo lattice reported in CeRuPO[28,29] and RENiAsO,[24] where the local criticality of 4f electrons mainly determine the intrinsic properties.

We prepared a series of Cu-doped $RE_2Ni_5As_3O_2$ samples to investigate the structure variation and superconductivity. The PXRD patterns and structural information is shown in Figures S4 and S5 and Table S1. Figure 6 presents the structural evolution of Cu-doped $RE_2Ni_5As_3O_2$ samples and the results are analogous to those of superconducting (La, Pr, Nd)$_2$(Ni$_{1-x}$Cu$_x$)$_5$As$_3$O$_2$ (x = 0.0−1.0). The a-lattice increases, while the c-lattice slightly decreases as $x < 0.6$. Once $x > 0.6$, the a-lattice decreases, while the c-axis rapidly increases, see Figure 6a,b. Figure 6c displays that the minima of c/a ratios show up at x = 0.6, where these minima are close to 5.45. Even though there are anomalies in lattice constants, the volumes of unit cell linearly increase by 3.6 and 4.2%, respectively, as shown in Figure 6d. Overall, the structural trend against Cu doping is similar to that of full solid solutions of $La_2(Ni_{1-x}Cu_x)_5As_3O_2$. However, the single-phase limits of solid solutions are 90 and 80% for Cu-doped $Ce_2Ni_5As_3O_2$ and $Sm_2Ni_5As_3O_2$, respectively.

Since the coordination environment of Ni and As is similar to that of FeAs-based superconductors, we summarize the Ni−As bond lengths, bond angles (Ni−As−Ni), and As height in the (Ni/Cu)$_5$As$_3$ unit of $RE_2(Ni_{1-x}Cu_x)_5As_3O_2$ (RE = Ce, Sm) compounds. The structure of (Ni/Cu)As plane in ac-plane is

DOI: 10.1021/acs.inorgchem.8b03360
Inorg. Chem. 2019, 58, 2770−2776

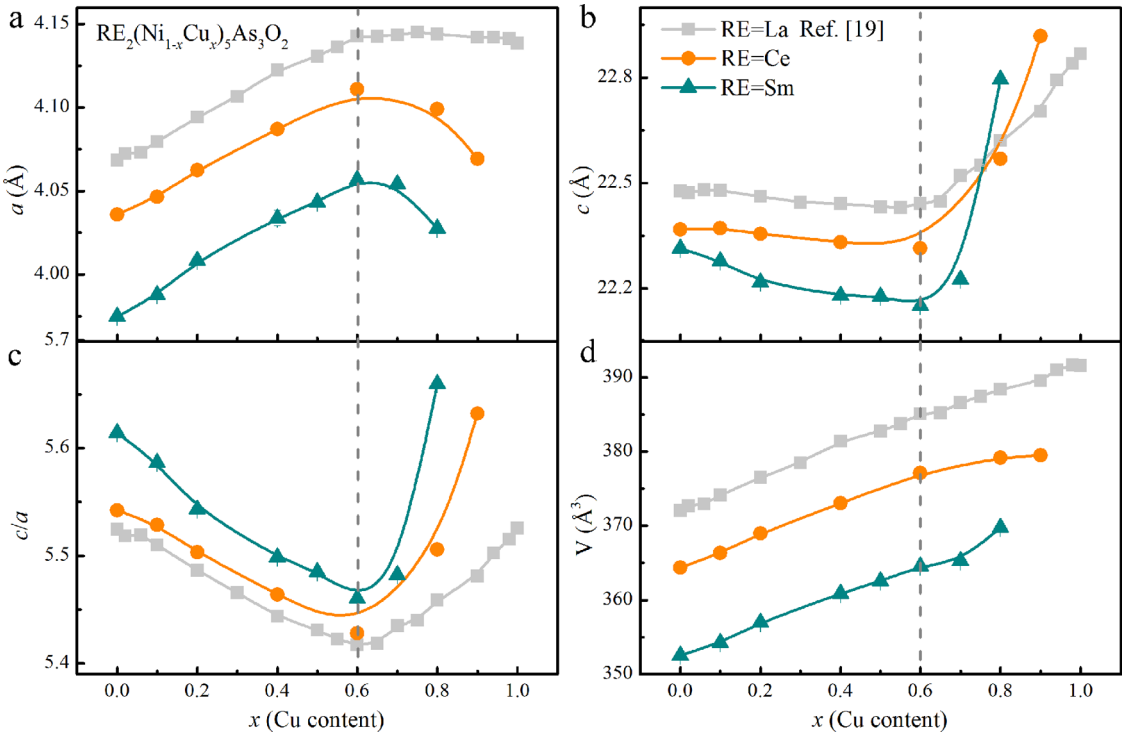

Figure 6. Lattice constants *a*, *c*, *c*/*a* ratio, and *V* of $RE_2(Ni_{1-x}Cu_x)_5As_3O_2$ as a function of Cu content.

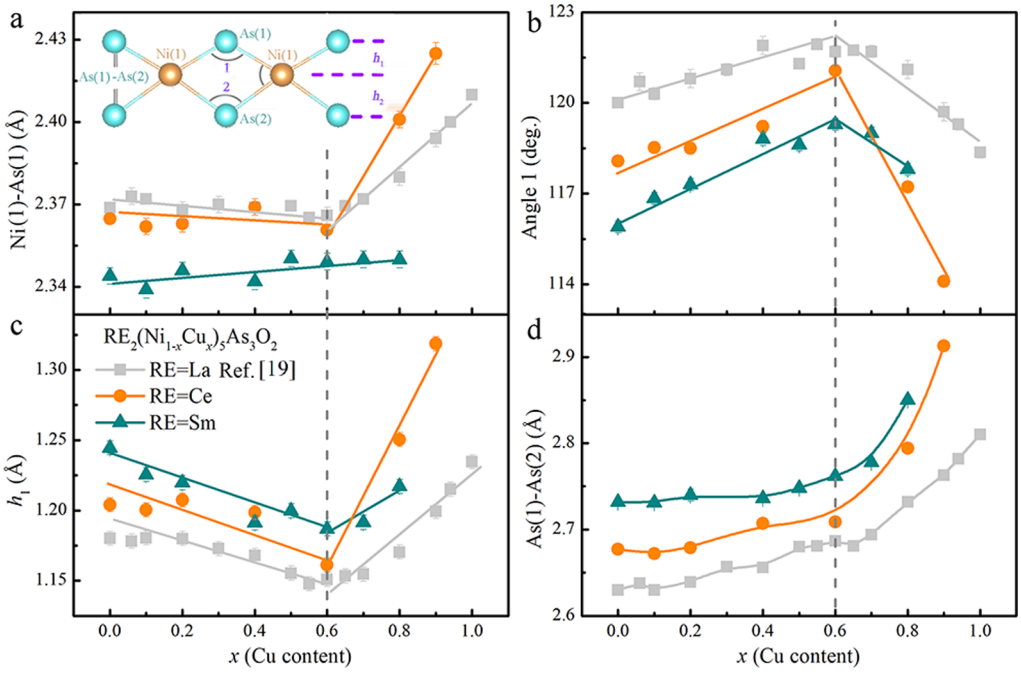

Figure 7. Cu-content-dependent Ni(1)−As(1) bond length (a), Ni(1)−As(1)−Ni(1) angle 1 (b), As height (h_1) (c), and As(1)−As(2) distance (d) in $RE_2(Ni_{1-x}Cu_x)_5As_3O_2$. Inset is structure of central CuAs fragment along *c*-axis.

shown in the inset Figure 7a. The anion heights (h_1 and h_2) are not identical due to different Wyckoff position of As(1) and As(2), which are synergistically determined by the Ni−As bond length and angles 1 and 2, respectively. From Figure 7a, one can see that the Cu doping slightly changes the Ni(1)−As(1) bond length $x < 0.6$, while it abruptly elongates the Ni(1)−As(1) bond lengths once $x > 0.6$. For $Sm_2(Ni_{1-x}Cu_x)_5As_3O_2$, the Cu-doping mildly increase this bond length in whole doping range. For angle 1, see Figure 7b; the Cu-doping straightly increases the value, while the trend is inversed as $x > 0.6$. As for the anion height h_1, it first decreases as $x < 0.6$ and then drastically increases; see Figure 7c. However, h_2 monotonously increases in the whole range of Cu doping; see Figure S6. The distinct trends of h_1 and h_2 induce that the As(1)−As(2) distance initially increases and then rapidly increases once the *x* is above 0.6, as shown in Figure 7d. As in previous reports,[10] the As−As covalent bond length is around 2.7−2.9 Å. As $x > 0.8$, both As−As distances are above

DOI: 10.1021/acs.inorgchem.8b03360
Inorg. Chem. 2019, 58, 2770−2776

2.85 Å, leading to a rather weak bonding state. It means that the As−As bond gradually breaks against Cu doping. In $La_2(Ni_{1-x}Cu_x)_5As_3O_2$, the As−As bond lengths are smaller than 2.80 Å, where the bonding states are stable. However, as the calculation of molecular COHP, the Fermi level is just below the antibonding states. The As−As bonding energy are 3.01 and 2.66 eV per bond for $Ce_2Ni_5As_3O_2$ and $Sm_2Ni_5As_3O_2$, respectively; see Figure S7. Doping Cu would naturally upshift the Fermi level to the antibonding states of As−As bond, destabilizing the structure.

Figure 8 is electrical resistivity of $RE_2(Ni_{1-x}Cu_x)_5As_3O_2$ (RE = Ce, Sm) samples. Most samples show metallic behaviors, and

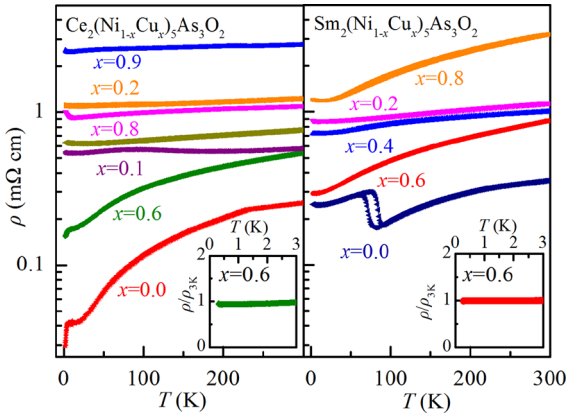

Figure 8. Temperature-dependent electrical resistivity (ρ) of $Ce_2(Ni_{1-x}Cu_x)_5As_3O_2$ and $Sm_2(Ni_{1-x}Cu_x)_5As_3O_2$. Insets are $\rho(T)/\rho(3\ K)$ for x = 0.6 samples from 0.25 to 3 K.

the resistivity jump due to phase transition in $RE_2(Ni_{1-x}Cu_x)_5As_3O_2$ is quickly suppressed by Cu doping. However, the low-temperature anomalies associated with AFM transition are still observed in $Ce_2(Ni_{1-x}Cu_x)_5As_3O_2$. Unfortunately, we did not see any superconductivity above 0.25 K in all measured samples, contrasting the findings in La/Pr/$Nd_2(Ni_{1-x}Cu_x)_5As_3O_2$ samples.

As we know, in the FeAs-based superconductors, the optimal h_1 and Fe−As−Fe angle 1 are 1.38 Å and 109.5°, respectively. Lowering (elevating) the h_1 would increase (decrease) the orbital hybridization and drive the system to more itinerant (localized) states, leading to suppression of T_c.[30] In the Ni_5As_3 unit, h_1 (1.17−1.31 Å) is apparently smaller than 1.38 Å, and angle 1 (115−120°) is larger than the empirically optimal value (109.5°), which may be the origin of itinerant states and lower T_c. However, we note that the h_1 and angle 1 in Ni_5As_3 are comparable to the counterparts of h_1 (1.13 and 1.15 Å) and the Ni−As−Ni angle (122.9 and 121.9°) in superconducting $AeNi_2As_2$ (Ae = Sr, Ba; T_c = 0.7 and 0.6 K) and LaNiAsO (2.4 K).[31−33] For $La_2(Ni_{1-x}Cu_x)_5As_3O_2$ superconductors, the sample with optimal T_c of 2.5 K has the smallest h_1 (1.15 Å) and the largest angle 1 (120.9°) at x = 0.6. Its h_1 can be easily tuned by Cu doping or changing RE^{3+} ions. Through Cu-doping, h_1 increases, and angle 1 decreases, which lower the T_c. Similarly, replacing the RE^{3+} ions by Sm^{3+} elevates the h_1, which also can explain the reason for suppressing T_c.

CONCLUSION

In summary, detailed structure analyses reveal there is optimal (Ni/Cu)As_4 geometry with As height (1.15 Å) and angle 1 (121.6°) for SC in $La_2(Ni_{1-x}Cu_x)_5As_3O_2$, which are far from the ideal values (1.38 Å and 109.5°) in FeAs-superconductors. Although the Cu substitution in antiferromagnetic (Ce/$Sm)_2(Ni_{1-x}Cu_x)_5As_3O_2$ could realize the more regular (Ni/Cu)As_4 tetrahedral, the SC is absent. From this point of view, the findings in Cu-doped $RE_2Ni_5As_3O_2$ apparently do not obey those empirical rules in FeAs-based superconductors. It provides a new perspective to fully understand the TM-based oxypnictides superconductors.

ASSOCIATED CONTENT

Supporting Information

The Supporting Information is available free of charge on the ACS Publications website at DOI: 10.1021/acs.inorgchem.8b03360.

Crystallographic parameters, PXRD patterns, −COHP (PDF)

AUTHOR INFORMATION

Corresponding Authors

*E-mail: jgguo@iphy.ac.cn.

*E-mail: xlchen@iphy.ac.cn.

ORCID

Xu Chen: 0000-0003-3477-2204

Jian-gang Guo: 0000-0003-3880-3012

Xiaolong Chen: 0000-0001-8455-2117

Notes

The authors declare no competing financial interest.

ACKNOWLEDGMENTS

This work was supported by the National Natural Science Foundation of China (No. 51772322 and 51532010), the National Key Research and Development Program of China (No. 2017YFA0304700 and 2016YFA0300600), and the Strategic Priority Research Program and Key Research Program of Frontier Sciences of the Chinese Academy of Sciences (No. XDB07020100 and QYZDJ-SSW-SLH013).

REFERENCES

(1) Lee, C. H.; Iyo, A.; Eisaki, H.; Kito, H.; Fernandez-Diaz, M. T.; Ito, T.; Kihou, K.; Matsuhata, H.; Braden, M.; Yamada, K. Effect of structural parameters on superconductivity in fluorine-free LnFeAsO$_{1-y}$ (Ln = La, Nd). *J. Phys. Soc. Jpn.* **2008**, *77*, No. 083704.

(2) Zhao, J.; Huang, Q.; de la Cruz, C.; Li, S. L.; Lynn, J. W.; Chen, Y.; Green, M. A.; Chen, G. F.; Li, G.; Li, Z.; Luo, J. L.; Wang, N. L.; Dai, P. C. Structural and magnetic phase diagram of $CeFeAsO_{1-x}F_x$ and its relation to high-temperature superconductivity. *Nat. Mater.* **2008**, *7*, 953.

(3) Zhang, C. L.; Harriger, L. W.; Yin, Z. P.; Lv, W. C.; Wang, M. Y.; Tan, G. T.; Song, Y.; Abernathy, D. L.; Tian, W.; Egami, T.; Haule, K.; Kotliar, G.; Dai, P. C. Effect of pnictogen height on spin waves in iron pnictides. *Phys. Rev. Lett.* **2014**, *112*, 217202.

(4) Kamihara, Y.; Watanabe, Y. T.; Hirano, M.; Hosono, H. Iron-based layered superconductor La[$O_{1-x}F_x$]FeAs (x = 0.05−0.12) with T_c = 26 K. *J. Am. Chem. Soc.* **2008**, *130*, 3296.

(5) Ren, Z. A.; Lu, W.; Yang, J. W.; Yi, X.; Xiao-Li, S.; Zheng-Cai; Guang-Can, C.; Shen, L.; Li, Z. C.; Che, G. C.; Dong, X. L.; Sun, L. L.; Zhou, F.; Zhao, Z. X. Superconductivity at 55K in iron-based F-doped layered quaternary compound Sm[$O_{1-x}F_x$]FeAs. *Chin. Phys. Lett.* **2008**, *25*, 2215.

(6) Chen, X. H.; Wu, T. G.; Wu, R.; Liu, H.; Chen, H.; Fang, D. F. Superconductivity at 43 K in $SmFeAsO_{1-x}F_x$. *Nature* **2008**, *453*, 761.

(7) Fujioka, M.; Denholme, S. J.; Ozaki, T.; Okazaki, H.; Deguchi, K.; Demura, S.; Hara, H.; Watanabe, T.; Takeya, H.; Yamaguchi, T.; Kumakura, H.; Takano, Y. Phase diagram and superconductivity at

DOI: 10.1021/acs.inorgchem.8b03360
Inorg. Chem. 2019, 58, 2770−2776

58.1 K in α-FeAs-free $SmFeAsO_{1-x}F_x$. *Supercond. Sci. Technol.* **2013**, *26*, No. 085023.
(8) Qi, Y. P.; Matsuishi, S.; Guo, J. G.; Mizoguchi, H.; Hosono, H. Superconductivity in defective pyrite-type iridium chalcogenides Ir_xCh_2 (Ch = Se and Te). *Phys. Rev. Lett.* **2012**, *109*, 217002.
(9) Hirai, D.; Von Rohr, F.; Cava, R. J. Emergence of superconductivity in $BaNi_2(Ge_{1-x}P_x)_2$ at a structural instability. *Phys. Rev. B: Condens. Matter Mater. Phys.* **2012**, *86*, 100505.
(10) Jia, S.; Jiramongkolchai, P.; Suchomel, M. R.; Toby, B. H.; Checkelsky, J. G.; Ong, N. P.; Cava, R. J. Ferromagnetic quantum critical point induced by dimer-breaking in $SrCo_2(Ge_{1-x}P_x)_2$. *Nat. Phys.* **2011**, *7*, 207.
(11) Guo, J. G.; Qi, Y. P.; Matsuishi, S.; Hosono, H. T_c maximum in solid solution of pyrite $IrSe_2$−$RhSe_2$ induced by destabilization of anion dimers. *J. Am. Chem. Soc.* **2012**, *134*, 20001.
(12) Guo, J. G.; Qi, Y. P.; Hosono, H. Structure and superconductivity in pyrite $Ir_{0.95-x}Rh_xTe_2$: A comparison with analogous selenides. *Phys. Rev. B: Condens. Matter Mater. Phys.* **2013**, *87*, 224504.
(13) Kudo, K.; Ishii, H.; Takasuga, M.; Iba, K.; Nakano, S.; Kim, J.; Fujiwara, A.; Nohara, M. Superconductivity induced by breaking Te_2 dimers of $AuTe_2$. *J. Phys. Soc. Jpn.* **2013**, *82*, No. 063704.
(14) Kitagawa, S.; Kotegawa, H.; Tou, H.; Ishii, H.; Kudo, K.; Nohara, M.; Harima, H. Pressure-induced superconductivity in mineral calaverite $AuTe_2$. *J. Phys. Soc. Jpn.* **2013**, *82*, 113704.
(15) Katayama, N.; Kudo, K.; Onari, S.; Mizukami, T.; Sugawara, K.; Sugiyama, Y.; Kitahama; Iba, Y. K.; Fujimura, K.; Nishimoto, N.; Nohara, M.; Sawa, H. Superconductivity in $Ca_{1-x}La_xFeAs_2$: a novel 112-type iron pnictide with arsenic zigzag bonds. *J. Phys. Soc. Jpn.* **2013**, *82*, 123702.
(16) Yakita, H.; Ogino, H.; Okada, T.; Yamamoto, A.; Kishio, K.; Tohei, T.; Ikuhara, Y.; Gotoh, Y.; Fujihisa, H.; Kataoka, K.; Eisaki, H.; Shimoyama, J. A new layered iron arsenide superconductor: $(Ca,Pr)FeAs_2$. *J. Am. Chem. Soc.* **2014**, *136*, 846.
(17) Ni, N.; Allred, J. M.; Chan, B. C.; Cava, R. J. High T_c electron doped $Ca_{10}(Pt_3As_8)(Fe_2As_2)_5$ and $Ca_{10}(Pt_4As_8)(Fe_2As_2)_5$ superconductors with skutterudite intermediary layers. *Proc. Natl. Acad. Sci. U. S. A.* **2011**, *108*, E1019−E1026.
(18) Löhnert, C.; Stürzer, T.; Tegel, M.; Frankovsky, R.; Friederichs, G.; Johrendt, D. Superconductivity up to 35 K in the iron platinum arsenides $(CaFe_{1-x}Pt_xAs)_{10}Pt_{4-y}As_8$ with layered structures. *Angew. Chem., Int. Ed.* **2011**, *50*, 9195.
(19) Chen, X.; Guo, J. G.; Gong, C. S.; Cheng, E. J.; Le, C. C.; Liu, N.; Ying, T. P.; Zhang, Q. H.; Hu, J. P.; Li, S. Y.; Chen, X. L. *c*-Axis dimer inducing dome-like superconductivity in weakly correlated $RE_2Cu_5As_3O_2$ (RE = La, Pr). arXiv:1808.06857.
(20) Rodríguez-Carvajal, J. Abstract of the satellite meeting on powder diffraction of the XV congress of the IUCr, Toulouse, France, 1990.
(21) Dronskowski, R.; Blöchl, P. E. Crystal orbital Hamilton populations (COHP): energy-resolved visualization of chemical bonding in solids based on density-functional calculations. *J. Phys. Chem.* **1993**, *97*, 8617−8624.
(22) Maintz, S.; Deringer, V. L.; Tchougréeff, A. L.; Dronskowski, R. LOBSTER: A tool to extract chemical bonding from plane-wave based DFT. *J. Comput. Chem.* **2016**, *37*, 1030−1035.
(23) Dai, P. C.; Hu, J. P.; Dagotto, E. Magnetism and its microscopic origin in iron-based high-temperature superconductors. *Nat. Phys.* **2012**, *8*, 709.
(24) Li, Y. K.; Luo, Y. K.; Li, L.; Chen, B.; Xu, X. F.; Dai, J. H.; Yang, X. J.; Zhang, Li.; Cao, G. H.; Xu, Z. A. Kramers non-magnetic superconductivity in LnNiAsO superconductors. *J. Phys.: Condens. Matter* **2014**, *26*, 425701.
(25) Qiu, Y.; Bao, W.; Huang, Q.; Yildirim, T.; Simmons, J. M.; Green, M. A.; Lynn, J. W.; Gasparovic, Y. C.; Li, J.; Wu, T.; Wu, G.; Chen, X. H. Crystal structure and antiferromagnetic order in $NdFeAsO_{1-x}F_x$ (x = 0.0 and 0.2) superconducting compounds from neutron diffraction measurements. *Phys. Rev. Lett.* **2008**, *101*, 257002.
(26) Jesche, A.; krellner, C.; de Souza, M.; Lang, M.; Geibel, C. Rare earth magnetism in CeFeAsO: a single crystal study. *New J. Phys.* **2009**, *11*, 103050.
(27) Neilson, J. R.; McQueen, T. M.; Llobet; Wen; Suchomel. Charge density wave fluctuations, heavy electrons, and superconductivity in KNi_2S_2. *Phys. Rev. B: Condens. Matter Mater. Phys.* **2013**, *87*, No. 045124.
(28) Krellner, C.; Kini, N. S.; Brüning, E. M.; Koch, K.; Rosner, H.; Nicklas, M.; Baenitz, M.; Geibel, C. CeRuPO: A rare example of a ferromagnetic Kondo lattice. *Phys. Rev. B: Condens. Matter Mater. Phys.* **2007**, *76*, 104418.
(29) Kitagawa, S.; Ishida, K.; Nakamura, T.; Matoba, M.; Kamihara, Y. Ferromagnetic quantum critical point in heavy-fermion iron oxypnictide $Ce(Ru_{1-x}Fe_x)PO$. *Phys. Rev. Lett.* **2012**, *109*, 227004.
(30) Kuroki, K.; Usui, H.; Onari, S.; Arita, R.; Aoki, H. Pnictogen height as a possible switch between high-T_c nodeless and low-T_c nodal pairings in the iron-based superconductors. *Phys. Rev. B: Condens. Matter Mater. Phys.* **2009**, *79*, 224511.
(31) Ronning, F.; Kurita, N.; Bauer, E. D.; Scott, B. L.; Park, T.; Klimczuk, T.; Movshovich, R.; Thompson, J. D. The first order phase transition and superconductivity in $BaNi_2As_2$ single crystals. *J. Phys.: Condens. Matter* **2008**, *20*, 342203.
(32) Bauer, E. D.; Ronning, F.; Scott, B. L.; Thompson, J. D. Superconductivity in $SrNi_2As_2$ single crystals. *Phys. Rev. B: Condens. Matter Mater. Phys.* **2008**, *78*, 172504.
(33) Watanabe, T.; Yanagi, H.; Kamihara, Y.; Kamiya, T.; Hirano, M.; Hosono, H. Nickel-based layered superconductor, LaNiOAs. *J. Solid State Chem.* **2008**, *181*, 2117−2120.

DOI: 10.1021/acs.inorgchem.8b03360
Inorg. Chem. 2019, 58, 2770−2776